

# Intermediate mass excess of dilepton production in heavy ion collisions at BEVALAC energies\*

C. Ernst<sup>†</sup>, S. A. Bass, M. Belkacem,

H. Stöcker and W. Greiner

*Institut für Theoretische Physik, J. W. Goethe-Universität*

*D-60054 Frankfurt am Main, Germany*

(December 2, 2024)

Dielectron mass spectra are examined for various nuclear reactions recently measured by the DLS collaboration. A detailed description is given of all dilepton channels included in the transport model UrQMD 1.0, i.e. Dalitz decays of  $\pi^0, \eta, \omega, \eta'$  mesons and of the  $\Delta(1232)$  resonance, direct decays of vector mesons and  $pn$  bremsstrahlung. The microscopic calculations reproduce data for light systems fairly well, but tend to underestimate the data in  $pp$  at high energies and in  $pd$  at low energies. These conventional sources, however, cannot explain the recently reported enhancement for nucleus-nucleus collisions in the mass region  $0.15 \text{ GeV} \leq M_{e^+e^-} \leq 0.6 \text{ GeV}$ . Chiral scaling and  $\omega$  meson broadening in the medium are investigated as a source of this mass excess. They also cannot explain the recent DLS data.

---

\*Supported by Graduiertenkolleg Theoretische und Experimentelle Schwerionenphysik, GSI, BMBF and DFG

<sup>†</sup>e-mail: ernst@th.physik.uni-frankfurt.de

## I. INTRODUCTION

Dileptons have been proposed in the late 70's as penetrating probes [1] of hot and dense nuclear systems. They are presumably created in all stages of heavy ion reactions by several distinct mechanisms. Once produced, they practically do not interact with the surrounding hadronic matter. Low mass dileptons are of particular interest (see e.g. [2–7]). They can reveal information of the *hadronic* properties in the reaction zone. Several experiments have focused on low mass lepton pairs: the DLS spectrometer at the BEVALAC [8,9], the CERES and HELIOS detectors at the SPS at CERN [10]. The dilepton spectrometers HADES at SIS at GSI [11] and PHENIX at RHIC in BNL [12] are under construction. The most striking result of the high energy dilepton programs so far is the observed enhancement in heavy systems at low invariant masses as compared to "conventional" hadronic cocktails and models. A dropping mass [13,14] or dissolving spectral function [15,16] of the  $\rho$  meson have been offered in attempt to explain these data. Recently, a systematic measurement of dilepton production at BEVALAC energies has been published. Data are available for elementary  $pp$  and  $pd$  collisions as well as for nucleus-nucleus collisions [8,9].

The aim of the present work is to investigate dilepton production within the microscopic  $n$ -body transport model UrQMD. The outline of the paper is as follows: In section II a brief survey of the UrQMD model is given. A more detailed description of the implemented dilepton production mechanisms follows. Section III contains the calculations of the elementary  $pp$  and  $pd$  dilepton cross sections in comparison to recent DLS measurements. Section IV shows mass spectra for heavier systems. Summary and concluding remarks are given in section V.

## II. PRODUCTION OF RESONANCES AND DILEPTONS

## A. Hadron production in the UrQMD model

The UrQMD model is based on the quantum molecular dynamics concept [17–19]. The Hamilton’s equations of motion are solved for gaussian wave packets. The model allows for the production of all established meson and baryon resonances up to about 2 GeV with all corresponding isospin projections and antiparticle-states. The collision term describes particle production by resonant excitation channels and, for higher masses, within a string fragmentation scheme. The UrQMD model is designed to cover consistently the whole range of bombarding energies per nucleon from 200 MeV to 200 GeV. For dilepton production at BEVALAC energies, the resonant production of neutral mesons is most important. A detailed description of the model can be found in refs. [20,21].

The formation of light mesons at low energies is modelled as a multistep process that proceeds via intermediate heavy baryon and meson resonances and their subsequent decay [22]. The resonance parameters (pole masses, widths and branching ratios) are taken from [23], but large uncertainties of these parameters are used to obtain a consistent fit to cross section data. For example, the production of  $\omega$  mesons is described in the UrQMD model by the formation and the decay of the  $N^*(1900)$  resonance. It decays to 35% into  $N\pi$  and to 55% into  $N\omega$ . As suggested in ref. [24], the  $\eta$  production proceeds not only via  $N^*(1535)$ , but invokes also nucleon resonances with masses 1650, 1700, 1710 and 2080 MeV. A full list of the UrQMD resonance parameters is published in ref. [20].

Broad resonances have mass dependent decay widths. For the resonance cross sections in baryon-baryon, meson-baryon and meson-meson collisions conventional Breit-Wigner parametrisations are used with mass dependent widths. At higher energies, the resonant particle production does no longer predict the observed cross sections. There, the string picture, described in [21], is employed.

Fig. 1 shows calculations of exclusive ( $pp \rightarrow mpp$ ) and inclusive ( $pp \rightarrow mX$ ) cross sections for the production of neutral mesons  $m = \pi^0, \eta, \rho^0, \omega$ . Recent data on the exclusive  $\eta$  production just above threshold are reproduced reasonably well [25]. Note that above 3.5 GeV the exclusive cross sections become less important, because the string channels

open and allow for multiple resonance production. For the present article the relevant  $\sqrt{s}$  values are below 4 GeV, where so far no data on the inclusive channels are available.

## B. Dilepton radiation in UrQMD

Dileptons can be produced in hadronic decays and collisions. The mechanisms that are expected to dominate in the low mass region (with invariant dilepton masses below 1 GeV) are the Dalitz decays ( $A \rightarrow Be^+e^-$ ) of neutral mesons  $\pi^0, \eta, \eta', \omega$ , as well as the Dalitz decay of the  $\Delta(1232)$  resonance. Around their pole masses the direct decays ( $A \rightarrow e^+e^-$ ) of the vector mesons  $\rho^0, \omega$  and  $\phi$  are expected to dominate the spectrum. These modes are of special interest: the invariant mass of the dilepton equals the vector meson mass in the hot and dense medium. Also included in the present model calculation is the  $pn$  bremsstrahlung. It contributes especially at low bombarding energies. In accord with ref. [3], other sources like Dalitz decays of heavier resonances,  $pp$ ,  $\pi N$  bremsstrahlung etc. are neglected for the reactions considered here. Direct dilepton production in binary collisions, e.g.  $\pi^+\pi^-, K^+K^- \rightarrow e^+e^-$  or  $\pi\rho \rightarrow e^+e^-$ , is not evaluated. In the framework of the present model this would correspond to a partial double counting: these reactions are supposedly included as explicit multi-step processes (e.g.  $\pi\rho \rightarrow \phi \rightarrow e^+e^-$ ). This also holds for the Dalitz decay of the  $a_1 \rightarrow \pi\rho \rightarrow \pi e^+e^-$ . At higher bombarding energies, however, direct processes like  $\pi\rho \rightarrow \pi e^+e^-$  might significantly contribute to the dilepton yield [26].

### 1. Dalitz decays of mesons

Decays of the type  $A \rightarrow Be^+e^-$  are not real multi body decays (for which usually the name Dalitz is used) but can be reduced to a decay into  $B$  plus a virtual photon (with an invariant mass  $M$ ) and subsequent conversion of the latter. Thus the matrix element factorises [27,28]

$$|\mathcal{M}|^2 = |\mathcal{M}(A \rightarrow B\gamma^*)|^2 \frac{1}{M^4} |\mathcal{M}(\gamma^* \rightarrow e^+e^-)|^2 . \quad (1)$$

This reflects in the differential decay rate, which can be written as a product of the conversion rate of the virtual gamma [29] and the decay width  $\Gamma_{A \rightarrow B\gamma^*}$  of  $A$  into a massive photon:

$$\frac{d\Gamma_{A \rightarrow Be^+e^-}}{dM} = \frac{2\alpha}{3\pi M} \sqrt{1 - \frac{4m_e^2}{M^2}} \left(1 + \frac{2m_e^2}{M^2}\right) \Gamma_{A \rightarrow B\gamma^*} . \quad (2)$$

Here  $m_e$  is the lepton mass. If one assumes that  $A$  decays isotropically in its restframe the  $A \rightarrow B\gamma^*$  width is given by

$$\Gamma_{A \rightarrow B\gamma^*} = \frac{|\vec{p}_{cm}|}{8\pi m_A^2} |\mathcal{M}_{A \rightarrow B\gamma^*}|^2 . \quad (3)$$

Here  $|\vec{p}_{cm}|$  is the decay momentum

$$|\vec{p}_{cm}| = \frac{\lambda^{\frac{1}{2}}(m_A^2, m_B^2, M^2)}{2m_A} \quad (4)$$

with the kinematic function  $\lambda(x^2, y^2, z^2) = (x^2 - (y + z)^2)(x^2 - (y - z)^2)$ .

A remaining difficulty resides in the calculation of the matrix element of the  $A \rightarrow B\gamma^*$  decay. The meson decays considered here are either of the type a) pseudoscalar ( $\pi^0, \eta, \eta'$ ) into a vector particle ( $\gamma$ ) plus a virtual photon or b) vector meson ( $\omega$ ) into a pseudoscalar meson plus a virtual photon. In both cases one gets [30]

$$|\mathcal{M}_{A \rightarrow B\gamma^*}|^2 = \frac{1}{2} |f_{AB}(M^2)|^2 \lambda(m_A^2, m_B^2, M^2) . \quad (5)$$

The form factor  $f_{AB}(M^2)$  is introduced to account for the strong interaction part of the vertex. It is common to normalise to the decay width into real photons [30] by dividing

$$\Gamma_{A \rightarrow B\gamma} = \frac{(m_A^2 - m_B^2)^3}{32\pi m_A^3} |f_{AB}(0)|^2 , \quad (6)$$

which re-expresses the form factors to  $F_{AB}(M^2) = \frac{f_{AB}(M^2)}{f_{AB}(0)}$ .

The form factors can be obtained from the vector meson dominance model (VMD). In the present calculations the following parametrisations are employed [28,6]

$$F_{\pi^0}(M^2) = 1 + b_{\pi^0} M^2$$

$$F_{\eta}(M^2) = \left(1 - \frac{M^2}{\Lambda_{\eta}^2}\right)^{-1}$$

$$\begin{aligned}
|F_\omega(M^2)|^2 &= \frac{\Lambda_\omega^2(\Lambda_\omega^2 + \gamma_\omega^2)}{(\Lambda_\omega^2 - M^2)^2 + \Lambda_\omega^2\gamma_\omega^2} \\
|F_{\eta'}(M^2)|^2 &= \frac{\Lambda_{\eta'}^2(\Lambda_{\eta'}^2 + \gamma_{\eta'}^2)}{(\Lambda_{\eta'}^2 - M^2)^2 + \Lambda_{\eta'}^2\gamma_{\eta'}^2}
\end{aligned} \tag{7}$$

with  $b_{\pi^0} = 5.5 \text{ GeV}^{-2}$ ,  $\Lambda_\eta = 0.72 \text{ GeV}$ ,  $\Lambda_\omega = 0.65 \text{ GeV}$ ,  $\gamma_\omega = 0.04 \text{ GeV}$ ,  $\Lambda_{\eta'} = 0.76 \text{ GeV}$  and  $\gamma_{\eta'} = 0.10 \text{ GeV}$ .

## 2. Delta Dalitz decay

The situation is more complicated for the Dalitz decay of the  $\Delta(1232)$  resonance. To complete eqs. (2) and (3), the matrix element for the process  $\Delta \rightarrow N\gamma^*$  has to be calculated. The corresponding interaction vertex has been analysed by Jones and Scadron [31] in the form

$$\mathcal{L}_{int} = e\bar{\Psi}_\beta\Gamma^{\beta\mu}A_\mu\psi + h.c. , \tag{8}$$

where  $\psi$ ,  $\Psi_\beta$  and  $A_\mu$  represent the fields of the nucleon, of the delta and of the photon, respectively. The dominant magnetic dipole transition yields the vertex function

$$\Gamma^{\beta\mu} = G_M(M^2)\frac{-3(m_\Delta + m_N)}{2m_N((m_\Delta + m_N)^2 - M^2)}\left(-m_\Delta\chi_1^{\beta\mu}\gamma_5 + \chi_2^{\beta\mu}\gamma_5 + \frac{1}{2}\chi_3^{\beta\mu}\gamma_5\right). \tag{9}$$

The choice of the  $\chi$  bears some freedom if only current conservation is ensured ( $q_\beta\Gamma^{\beta\mu} = 0$ ). Following ref. [31], one may write

$$\begin{aligned}
\chi_1^{\beta\mu} &= (q^\beta\gamma^\mu - q \cdot \gamma g^{\beta\mu}) , \\
\chi_2^{\beta\mu} &= (q^\beta P^\mu - q \cdot P g^{\beta\mu}) , \\
\chi_3^{\mu\beta} &= (q^\beta q^\mu - q^2 g^{\beta\mu}) ,
\end{aligned} \tag{10}$$

with  $P = 1/2(p_\Delta + p_N)$  and  $q = p_\Delta - p_N$ .  $G_M$  in eq. (9) stands for the magnetic dipole form factor. It can be fixed at  $M = 0$  to the decay into a real photon, yielding  $G_M(0) = 3.0$ . The  $M$ -dependence of the overall form factor is subject to speculation: the time-like electromagnetic form factors for baryons are unknown in the kinematic region of

interest. In the present calculations any VMD-type form factors are omitted. This gives a lower limit for the  $\Delta$  Dalitz contribution in the region of the vector meson poles.

Using eqs. (8,9), we can express the matrix element via

$$\hat{\mathcal{M}}_i = e\bar{u}_\beta(p_\Delta, s_\Delta)\chi_i^{\beta\mu}\gamma_5\epsilon_\mu(p_\gamma, s_\gamma)u(p_N, s_N). \quad (11)$$

The matrix element may be written as a linear combination of the  $\hat{\mathcal{M}}_i$  and  $\hat{\mathcal{M}}_j^*$ :

$$|\mathcal{M}|^2 = e^2 G_M^2 \frac{9(m_\Delta + m_N)^2}{4m_N^2((m_\Delta + m_N)^2 - M^2)^2} \sum_{i,j=1}^3 c_i \hat{\mathcal{M}}_i c_j \hat{\mathcal{M}}_j^*, \quad (12)$$

where  $c_1 = -m_\Delta$ ,  $c_2 = 1$  and  $c_3 = 1/2$ . The appearing traces have been calculated using the *Mathematica* package HIP [32]. One then obtains:

$$\begin{aligned} \sum_{i,j=1}^3 c_i \hat{\mathcal{M}}_i c_j \hat{\mathcal{M}}_j^* &= \frac{1}{9} \left( (m_\Delta - m_N)^2 - M^2 \right) \\ &\times \left( 7m_\Delta^4 + 14m_\Delta^2 M^2 + 3M^4 + 8m_\Delta^3 m_N + 2m_\Delta^2 m_N^2 + 6M^2 m_N^2 + 3m_N^4 \right). \end{aligned} \quad (13)$$

Substituting eqn. (12) and (13) into eq. (3), we get the  $\Delta$  Dalitz decay width.

Fig. 2 shows the differential mass distributions of the Dalitz decay probabilities as implemented into the UrQMD model. While the very low masses are dominated by  $\pi^0$  and  $\eta$  decays, the  $\omega$  and  $\eta'$  decays are more important at higher masses. The contributions of the  $\Delta$  decays are also shown for different masses of the  $\Delta(1232)$ . Heavy  $\Delta$ 's naturally contribute more to the probabilities than lighter ones. In calculating the dilepton spectrum these probabilities are multiplied with the yields of the corresponding particle species. At low energies the dominant  $\pi N \Delta$  system [18] can push the  $\Delta$  contributions over those of the heavy mesons. On the other hand, the small yield of the  $\eta'$  will make it invisible, due to the tremendous background of other sources in the relevant mass region.

### 3. Direct decays of vector mesons

The decay width of the electromagnetic two-body decays of the vector mesons are assumed (similar to ref. [6]) to be of the form

$$\Gamma_{V \rightarrow e^+e^-}(M) = \frac{c_V}{M^3} \sqrt{1 - \frac{4m_e^2}{M^2}} \left( 1 + \frac{2m_e^2}{M^2} \right) \Theta(M - 2m_e). \quad (14)$$

The constants  $c_V$  are fitted to yield the vacuum widths given in ref. [23] at the resonance poles. One obtains  $c_\rho = 3.079 \times 10^{-6} \text{ GeV}^4$ ,  $c_\omega = 0.287 \times 10^{-6} \text{ GeV}^4$  and  $c_\phi = 1.450 \times 10^{-6} \text{ GeV}^4$ .

It is assumed that vector mesons can radiate off dileptons continuously [33]. The dilepton mass distribution is given by the time-integral over the mass distributions of mesons plus an additional term which accounts for the decays after some typical freeze-out time  $t_f$  (the last term can be dropped if  $t_f \rightarrow \infty$ )

$$\frac{dN_{ee}}{dM} = \int_0^{t_f} dt \frac{dN_V(t)}{dM} \cdot \Gamma_{V \rightarrow ee}(M) + \frac{dN_V(t_f)}{dM} \cdot \frac{\Gamma_{V \rightarrow ee}(M)}{\Gamma_{V,tot}(t_f)}. \quad (15)$$

If absorption is negligible, this approach is equivalent to the method of adding one dilepton (with appropriate normalisation) at each decay vertex. However, this "shining" method gives a better sampling of the density probed by the hadron and thus a better statistics for density dependent spectral functions. In addition, there is generally a complicated time dependence of the total hadron width  $\Gamma_{tot}(t, \vec{r})$ , caused by the in-medium modifications of the quasiparticle widths. The approach eq. (15) has the advantage to be explicitly independent of the in-medium width, if  $t_f$  is reasonably high, so that the total width takes on it's vacuum properties.

#### 4. Incoherent bremsstrahlung

In the soft photon approximation (SPA) the cross section for real photons with four-momentum  $q^\mu$  in collisions  $a + b \rightarrow X$  can be expressed as

$$q_0 \frac{d\sigma_{ab}^{\gamma X}}{d^3q} = \frac{\alpha}{4\pi^2} |\epsilon \cdot J|^2 d\sigma_{ab}^X. \quad (16)$$

$d\sigma_{ab}^X$  denotes the differential cross section of the (strong)  $ab$  interaction without any photon in the final state.  $\epsilon$  is the polarisation vector of the photon. The current  $J^\mu$  is given by

$$J^\mu(q) = -Q_a \frac{p_a^\mu}{p_a \cdot q} - Q_b \frac{p_b^\mu}{p_b \cdot q} + \sum_{i=1}^X Q_i \frac{p_i^\mu}{p_i \cdot q}, \quad (17)$$

where the  $Q$ 's and  $p$ 's denote the charges and momenta of the corresponding particles.

The SPA is justified only for  $M, q_0 \rightarrow 0$ . To extrapolate to the case of hard and massive virtual photons, a phase space correction can be applied by multiplying the cross section with the ratio of the phase space integrals with/without a virtual photon [34]. Similarly to eq. (2) one gets

$$\frac{d\sigma_{ab}^{e^+e^-X}}{d^3q dM} = \frac{\alpha^2}{6\pi^3} \sqrt{1 - \frac{4m_e^2}{M^2}} \left(1 + \frac{2m_e^2}{M^2}\right) |\epsilon \cdot J|^2 \frac{R_n(\bar{s})}{R_n(s)} \frac{d\sigma_{ab}^X}{q_0 M}. \quad (18)$$

Here  $R_n$  is defined as

$$R_n(s) = \int d\Phi_n(s, p_1 \dots p_n), \quad (19)$$

where  $d\Phi_n$  is the volume element of the  $n$ -dimensional Lorentz invariant phase space and  $\bar{s}$  is the squared effective energy of the system after the emission of the  $\gamma^*$ ,

$$\bar{s} = s + M^2 - 2\sqrt{s}q_0. \quad (20)$$

The correction factor for two outgoing particles reads

$$\frac{R_2(\bar{s}, m_a^2, m_b^2)}{R_2(s, m_a^2, m_b^2)} = \frac{\lambda^{1/2}(\bar{s}, m_a^2, m_b^2) s}{\lambda^{1/2}(s, m_a^2, m_b^2) \bar{s}}. \quad (21)$$

Eq. (18) is a general expression for the bremsstrahlung dilepton production in the SPA. In the case of proton-neutron bremsstrahlung ( $pn \rightarrow p'n'\gamma^*$ ), the current is given by  $J^\mu = p_{p'}^\mu/q \cdot p_{p'} - p_p^\mu/q \cdot p_p$ . As a result we have

$$|\epsilon \cdot J|^2 = \frac{-t}{q_0^2 m_p^2}, \quad (22)$$

with the Mandelstam variable  $t = (p_p - p_{p'})^2$ . Then eq. (18) takes the form

$$\frac{d\sigma_{pn}^{pne^+e^-}}{d^3q dM} = \frac{\alpha^2}{6\pi^3} \sqrt{1 - \frac{4m_e^2}{M^2}} \left(1 + \frac{2m_e^2}{M^2}\right) \frac{\bar{\sigma}}{q_0^3 M} \frac{R_2(\bar{s})}{R_2(s)}. \quad (23)$$

Here  $\bar{\sigma}$  is the momentum-transfer weighted  $pn$  elastic cross section

$$\bar{\sigma} = \int_{-(s-4m_p^2)}^0 \left(\frac{-t}{m_p^2}\right) \frac{d\sigma}{dt} dt. \quad (24)$$

A proper parametrisation of  $\bar{\sigma}$  is rather important [35]. A systematic overestimation of the differential bremsstrahlung production results if the asymmetry of the momentum-transfer weighted cross section is not included. In the present work, a parametrisation similar to that of ref. [35] is used. It consists of a symmetric low energy part and an asymmetric high energy component.

Fig. 3 shows the cross section for  $pn \rightarrow pn + e^+e^-$  bremsstrahlung at different bombarding energies. Note that at low masses, the cross section is practically not sensitive to the incident energy. As a result, the  $pn$  bremsstrahlung is relatively unimportant as resonance channels become dominant at  $E_{kin} \sim 1.5$  GeV.

Bremsstrahlung from  $pp$  collisions is expected to be small at low energies due to destructive interferences. However, at the highest energies considered here, the  $pp$  bremsstrahlung contribution may be comparable to the  $pn$  bremsstrahlung yield [36]. On the other hand, the total contribution of bremsstrahlung is found to be negligible for all practical purposes at those energies (see sect. III B). Note that the SPA already gives an upper estimate of the expected dilepton yield [37].

### III. DILEPTON CROSS SECTIONS IN ELEMENTARY SYSTEMS

Before one can investigate the dilepton production in nucleus-nucleus reactions, one should first check the model in elementary  $pp$  and  $pd$  collisions. Recently, the DLS collaboration published a systematic study on dielectron cross sections in light systems for beam kinetic energies  $E_{kin}$  from 1 to 5 GeV. The corresponding centre-of-mass energies range from below the  $\eta$  production threshold up to 3.6 GeV, where phase space is wide open for the abundant production of a large variety of resonances.

The acceptance of the DLS does not cover the entire phase space. Thus the calculated dilepton pairs are corrected for the limited spectrometer acceptance region (DLS-filter V4.1). The finite mass resolution of  $\Delta M/M \approx 0.1$  is incorporated by folding the calculated spectra with a Gaussian of width  $\Delta M$ . The acceptance correction strongly influences the low-mass spectra while the mass resolution smoothing affects the shape of

the spectra at higher masses.

### A. $pp$

The resulting dilepton mass spectra for  $pp$  collisions are shown in fig. 4.

Only 0.46 GeV of c.m. energy are available for particle production at  $E_{kin} = 1.04$  GeV. Thus, only pion- and  $\Delta$ -Dalitz decays contribute in this case. The model satisfactorily reproduces the data at low masses, but underestimates them around  $M_{e^+e^-} = 0.4$  GeV. The disagreement could be caused by the abovementioned uncertainties in calculating the electromagnetic form factor of the  $\Delta N\gamma$  system. The first generation of DLS data was incompatible to free form factors [3,38]. This situation is now unclear, because the data of the second run tends to exceed the first. However, limited statistics and the better agreement at higher beam energies precludes a definite conclusion on the origin of the "enhancement" at  $E_{kin} = 1.04$  GeV.

At  $E_{kin} = 1.27 - 1.85$  GeV the model explains the data with growing influence of meson decays. One can see from fig. 4 that first the  $\eta$ -Dalitz decay and then the direct  $\rho$  and  $\omega$  decay become more important. In the UrQMD calculation of  $pp$ , most of the  $\rho^0$  ( $\approx 99\%$ ) are not created in  $\pi^+\pi^-$  collisions, but result from heavy baryon decays. The limited phase space at low c.m. energies [22] and the strong ( $M^{-3}$ ) mass dependence of the dilepton decay widths (14) are responsible for the deformation of the  $\rho$  spectrum towards low masses. The cross section for the Dalitz production through  $\Delta$  decays remains rather constant at low masses, with increasing energy, but increases towards higher masses. Indeed, it is known from  $pp \rightarrow n\Delta^{++}$  reactions, that heavier  $\Delta$ 's become more important with increasing beam energy due to the mass dependence of the decay widths [39]. In fact, there is a good agreement at intermediate beam energies (disregarding the data point at  $M_{e^+e^-} = 200$  MeV) which would be worsened if the electromagnetic  $\Delta N\gamma$  form factor would be included, in particular at  $E_{kin} \geq 1.6$  GeV.

The model does not reproduce the shape of the measured spectrum at  $E_{kin} = 2.1$  GeV and 4.9 GeV. Around  $M = 0.6$  GeV the ratio between the  $pp$  and  $pd$  data decreases for

the two highest beam energies. If this gets confirmed, it might be explainable by some strong contribution of  $pp$  bremsstrahlung, which was not considered here.

## B. $pd$

$pd$  calculations are shown in fig. 5. The calculated events are minimum-bias triggered at a maximum impact parameter of  $b = 1.6$  fm, i.e. a geometric cross section equal to the measured one of about 80 mb.

An important difference to the  $pp$  system is due to the internal motion of bound nucleons. This motion smears out the production thresholds. Consequently, one observes subthreshold contributions from  $\eta$  and  $\rho$  mesons already at  $E_{kin} = 1.04$  GeV.

Unlike in  $pp$  collisions, the proton-deuteron data overestimate the model results in the mass region dominated by the  $\eta$  decay. This indicates an asymmetry in the  $pp$  and  $pn$  production cross sections as predicted from one-boson exchange models [40]. Indeed, it was measured that just above the threshold, the ratio of  $pd$  to  $pp$  induced  $\eta$  cross sections is much larger than two [41]. However, due to the Fermi motion in the deuteron, it is not straight forward to extract  $pn$  cross sections from  $pp$  and  $pd$  measurements. On the other hand, direct measurements of the  $\eta$  production in  $pn$  are still not available. We have therefore evaluated the ratio  $R_\eta = \sigma(pd \rightarrow \eta X)/\sigma(pp \rightarrow \eta X)$  without any explicit modification of the  $pn$  cross section to estimate the influence of Fermi motion. At  $E_{kin} = 1.27$  GeV, close to threshold, we get the large value  $R_\eta = 17 \pm 3$  while above  $E_{kin} = 1.61$  GeV,  $R_\eta$  remains practically constant, between 2.8 and 2.3.

However, the large value of  $R_\eta$  is not enough to explain the integrated total dilepton ratios. This is shown in fig. 6 where

$$R = \frac{\int_{0.15 \text{ GeV}}^{M_{max}} \left( \frac{d\sigma_{pd}}{dM} \right) dM}{\int_{0.15 \text{ GeV}}^{M_{max}} \left( \frac{d\sigma_{pp}}{dM} \right) dM} \quad (25)$$

is plotted vs. the incident energy. The predicted dilepton ratios are rather low at energies smaller than 2 GeV. A similar behaviour is also found in BUU calculations [4], which include  $pp$  bremsstrahlung. This indicates that there is a common feature of known

transport models with "conventional" sources to underestimate the recent DLS nucleus-data at intermediate dilepton masses [8]. At  $E_{kin} = 1.27 \text{ GeV}$  the model predicts only  $R = 5.2$ . This value is lower than the corresponding one of  $R_\eta$ , because the  $\eta$  is yet only a marginal dilepton source at this energy.

Within the statistical uncertainties the mass-differential dilepton cross sections for  $pd$  can be explained by the model for the two highest beam energies. Note that  $pn$  bremsstrahlung is relatively unimportant.

#### IV. DILEPTONS IN HEAVY ION COLLISIONS

Fig. 7 compares the UrQMD predictions with DLS data for various nucleus-nucleus reactions [8]. At first glance the examined systems all exhibit a qualitatively similar behaviour in three distinct mass regions:

In the lowest mass region (up to 150 MeV) the spectrum is dominated by the pionic Dalitz decay. There are also strong effects of the acceptance filter, which significantly suppresses the low-mass yield (compare Fig. 2 for the shape of uncorrected Dalitz spectra). Other sources are of little importance in this mass region. However, near  $M = 150 \text{ MeV}$ , the  $\Delta$  Dalitz decay becomes more important.

At intermediate masses the data show a noticeable enhancement of the dilepton yield as compared to the model calculations. There is a considerable confusion about these recent data because the new yields strongly exceed earlier published measurements [42]. The latter have been revised by the DLS collaboration due to large, previously uncorrected trigger inefficiencies. However, the present calculations and, also, results of other models e.g. [3,43–45], are closer to the earlier measurements in the considered mass range (see fig. 8).

The theoretical spectrum at  $M > 600 \text{ MeV}$  is dominated by direct  $\rho^0$  and  $\omega$  decays. The model cross sections for dilepton production via  $\rho$  mesons nicely account for the data in this region. The two highest data points in He-Ca suffer from lack of statistics. For all nuclear systems, only about 50% of all  $\rho$  mesons stem from  $\pi^+\pi^-$  annihilations, the other

50% are produced in decays [22].

Turning back to the intermediate region, one sees a similar dilepton enhancement as in the  $pd$  data. There one may partially attribute the enhancement to the high  $pn \rightarrow \eta X$  cross section. Therefore, it seems reasonable to reproduce the data by artificially enhancing the  $\eta$  yield. We rescaled the  $\eta$  yield by a factor  $f_\eta$  and found good agreement both in shape and absolute yield with  $f_\eta \approx 10$  for C+C and  $\approx 20$  for Ca+Ca. However, this is not supported by TAPS data which found the  $4\pi$  extrapolated  $\eta$  cross section in Ca+Ca at 1 GeV to be about 20 mb [46]. Our rescaled cross section corresponds to  $\approx 120$  mb. A dropping  $\eta$  mass has been introduced in ref. [45] to explain the DLS data. But these studies also found the increased  $\eta$  cross sections to be incompatible to the TAPS measurements.

We note that the inclusion of a density-dependent  $\Delta N\gamma$  form factor for the  $\Delta$  Dalitz decay, as discussed in ref. [3], can give a sizeable enhancement of the calculated dilepton yield at intermediate masses  $0.2 \text{ GeV} < M < 0.6 \text{ GeV}$ . However, this is ruled out as an explanation, because the fair agreement of the calculation to the data in the high-mass region  $M > 600 \text{ MeV}$  would be destroyed by a strong overestimation.

Due to  $\sigma - \omega$  mixing via an  $NN^{-1}$  loop, the  $2\pi$  decay channel of the  $\omega$  might be significantly enhanced in nuclear matter [47]. To get an estimate for possible effects on intermediate mass lepton pairs, we have increased  $\Gamma_{\omega \rightarrow \pi\pi}$  by a factor of 500 to approximately 100 MeV. The solid curves in fig. 9 show the result of this calculation for the Ca+Ca system. As can be seen, the mass distribution of dilepton pairs from direct  $\omega$  decays becomes very broad. Nevertheless, this contribution has almost no effect on the total dilepton yield and does not suffice to explain the measured enhancement.

One approach to describe the density dependence of vector meson masses is the linear scaling law of Hatsuda and Lee [48]:

$$m_V^* = m_V(1 - 0.18\rho/\rho_0), \quad (26)$$

where  $\rho_{(0)}$  is the local (ground state) density and  $m_V^{(*)}$  is the (modified) vector meson mass. Although more sophisticated calculations predict a more complex behaviour of the vector meson spectral functions [15], the scaling law seems to be reasonable for the

effective masses. To check this idea using the UrQMD model, the poles of the produced quasi particle vector mesons have been shifted according to (26). One obtains the dashed curves in fig. 9. It is found that the dropping mass scenario – and also more complex in-medium spectral functions (see ref. [45]) – cannot account for the new DLS data.

## V. SUMMARY

Dilepton production has been studied within the microscopic non-equilibrium transport model UrQMD. The production mechanisms have been critically revisited. We have compared the model with the DLS data for  $pp$  and  $pd$  collisions at different beam energies. Resonance decays into dileptons were found to be able to explain the low energy  $pp$  data.

The UrQMD model predictions for the  $pd$  system are below the new DLS data for masses 0.3-0.6 GeV. A similar, but even stronger underestimation takes place in collisions of heavier nuclei. The present paper points out that the large enhancement in the data as compared to model calculations cannot be accounted for by two distinct hypotheses on the in-medium modifications of vector mesons. An enhancement of the  $\eta$  production in  $pn$  collisions is able to reproduce the yield and shape of the AA spectra. However, huge  $\eta$  production cross sections would be required, in contrast to TAPS data.

## ACKNOWLEDGEMENTS

C. E. wants to thank A. Dumitru, G. Mao, L. Satarov and L. Winkelmann for valuable discussions and H. S. Matis for providing the DLS acceptance filter.

- 
- [1] E. L. Feinberg, Nuovo Cim. **34A**, 391 (1976).  
 E. V. Shuryak, Phys. Lett. **B78**, 150 (1978).  
 G. Domokos and J. I. Goldman, Phys. Rev. **D23**, 203 (1981).
- [2] C. Gale and J. Kapusta, Nucl. Phys. **A471**, 35c (1987).

- [3] G. Wolf *et al.*, Nucl. Phys. **A517**, 615 (1990).
- [4] A. I. Titov, B. Kämpfer, and E. L. Bratkovskaya, Phys. Rev. **C51**, 227 (1995).
- [5] W. Cassing, W. Ehehalt, and C. M. Ko, Phys. Lett. **B363**, 35 (1995).
- [6] C. M. Ko, G. Q. Li, G. E. Brown, and H. Sorge, Nucl. Phys. **A610**, 342c (1996).
- [7] E. L. Bratkovskaya and W. Cassing, Nucl. Phys. **A619**, 413 (1997).
- [8] R. J. Porter *et al.*, Phys. Rev. Lett. **79**, 1229 (1997).
- [9] W. K. Wilson *et al.*, Phys. Rev. (1997).
- [10] A. Drees, Nucl. Phys. **A610**, 536c (1996).
- [11] J. Stroth *et al.*, Dilepton spectroscopy with HADES at SIS, in *Proc. of the International Workshop on Gross Properties of Nuclei and Nuclear Excitation, XXII, Hirschegg, Austria*, edited by H. Feldmeier and W. Nörenberg, 1995.
- [12] J. C. Gregory *et al.*, Nucl. Phys. **A566**, 287C (1994).
- [13] G. E. Brown and M. Rho, Phys. Rev. Lett. **66**, 2720 (1991).
- [14] T. Hatsuda and H. Shiomi, Nucl. Phys. **A590**, 545 (1995).
- [15] R. Rapp, G. Chanfray, and J. Wambach, Nucl. Phys. **A617**, 472 (1997).  
 F. Klingl, N. Kaiser, and W. Weise, (1997), hep-ph/9704398.  
 W. Peters, M. Post, H. Lenske, S. Leupold, and U. Mosel, (1997), nucl-th/9708004.
- [16] W. Cassing and E. L. Bratkovskaya, (1997), nucl-th/9708020.
- [17] J. Aichelin and H. Stöcker, Phys. Lett. **B176**, 14 (1986).  
 H. Sorge, H. Stöcker, and W. Greiner, Annals of Physics **192**, 266 (1989).  
 J. Aichelin, Phys. Rep. **202**, 233 (1991).
- [18] S. A. Bass, C. Hartnack, H. Stöcker, and W. Greiner, Phys. Rev. **C51**, 3343 (1995).
- [19] L. A. Winckelmann *et al.*, Nucl. Phys. **A610**, 116c (1996).

- [20] S. A. Bass *et al.*, to be published in Prog. Part. Nucl. Phys. (1998).
- [21] M. Bleicher *et al.*, to be published (1998).
- [22] L. A. Winckelmann, H. Sorge, H. Stöcker, and W. Greiner, Phys. Rev. **C51**, R9 (1995).
- [23] Particle Data Group, Phys. Rev. **D54**, 1 (1996).
- [24] M. Batinic, I. Slaus, A. Svarc, and B. M. K. Nefkens, Phys. Rev. **C51**, 2310 (1995).
- [25] H. Calen *et al.*, Phys. Lett. **B366**, 39 (1996).
- [26] J. Murray, W. Bauer, and K. Haglin, (1996), hep-ph/9611328.
- [27] N. S. Craigie, Phys. Rep. **47**, 1 (1978).
- [28] L. G. Landsberg, Phys. Rep. **128**, 301 (1985).
- [29] N. M. Kroll and W. Wada, Phys. Rev. **98**, 1355 (1955).
- [30] P. Koch, Z. Phys. **C57**, 283 (1993).
- [31] H. F. Jones and M. D. Scadron, Annals of Physics **81**, 1 (1973).
- [32] A. Hsieh and E. Yehudai, Comput. Phys. **6**, 253 (1992).
- [33] U. Heinz and K. S. Lee, Nucl. Phys. **A544**, 503c (1992).
- [34] C. Gale and J. Kapusta, Phys. Rev. **C40**, 2397 (1989).
- [35] L. A. Winckelmann, H. Stöcker, W. Greiner, and H. Sorge, Phys. Lett. **B298**, 22 (1993).
- [36] K. Haglin and C. Gale, Phys. Rev. **C49**, 401 (1994).  
J. Zhang, R. Tabti, C. Gale, and K. Haglin, J. Mod. Phys **E6**, 475.
- [37] P. Lichard, Phys. Rev. **D51**, 6017 (1995).
- [38] M. Schäfer, H. C. Dönges, A. Engel, and U. Mosel, Nucl. Phys. **A575**, 429 (1991).
- [39] V. Dmitriev, O. Sushkov, and C. Gaarde, Nucl. Phys. **A459**, 503 (1986).

- [40] T. Vetter, A. Engel, T. Biro, and U. Mosel, Phys. Lett. **B263**, 153 (1991).
- [41] E. Chiavassa *et al.*, Phys. Lett. **B337**, 192 (1994).
- [42] G. Roche *et al.*, Phys. Lett. **B226**, 228 (1989).
- [43] L. Xiong, Z. G. Wu, C. M. Ko, and J. Q. Wu, Nucl. Phys. **A512**, 772 (1990).
- [44] E. L. Bratkovskaya, W. Cassing, and U. Mosel, Phys. Lett. **B376**, 12 (1996).
- [45] E. L. Bratkovskaya, W. Cassing, R. Rapp, and J. Wambach, (1997), nucl-th/9710043.
- [46] F. D. Berg *et al.*, Phys. Rev. Lett. **72**, 977 (1994).
- [47] G. Wolf, B. Friman, and M. Soyeur, (1997), nucl-th/9707055.
- [48] T. Hatsuda and S. H. Lee, Phys. Rev. **C46**, R34 (1992).
- [49] V. Flaminio, W. G. Moorhead, D. R. O. Morrison, and N. Rivoire, CERN, Geneva Report No. CERN-HERA-84-01, 1984 (unpublished).

## FIGURE CAPTIONS

**FIG. 1** Cross sections for neutral meson production in  $pp$  collisions. Calculations are shown for the exclusive and inclusive production of  $\pi^0$ ,  $\eta$ ,  $\omega$  and  $\rho^0$  mesons in comparison to available data [49,25].

**FIG. 2** Differential probability distributions for Dalitz decays. The mass-differential branching ratios for decays of  $\pi^0$  (dashed),  $\eta$  (solid),  $\omega$  (long-dashed) and  $\eta'$  (dotted) mesons can be seen. Also shown is the parametrisation for Dalitz decays of the  $\Delta(1232)$  resonances at pole mass (dotted) and of a heavy  $\Delta(1232)$  with mass  $m_\Delta = 1.432$  GeV (dash-dotted).

**FIG. 3** Differential cross section for the production of a bremsstrahlung pair in elastic  $pn$  collisions for beam kinetic energies  $E_{kin} = 1.04$  (solid), 2.09 (dotted) and 4.88 GeV (dash-dotted).

**FIG. 4** The  $e^+e^-$  mass spectra for  $pp$  reactions at six kinetic energies. The upper solid curve is the sum of all contributions. One can see the contributions of  $\pi^0$  (dotted),  $\Delta$  (dash-dotted),  $\eta$  (dashed) and  $\omega$  (dotted) Dalitz decays as well as of the direct  $\rho^0$  (solid) and  $\omega$  (thin-solid) dilepton decays. Every single dilepton has passed the DLS Filter 4.1 and a mass resolution of 10% is adopted. The data are from [9].

**FIG. 5** Acceptance-corrected mass spectra for proton + deuterium. The individual sources are marked as in fig. 4, but there is an additional contribution from  $pn$  bremsstrahlung (thick-dotted).

**FIG. 6** Ratio of the integrated cross section for  $pd$  to  $pp$  reactions as a function of the beam energy. The solid line shows the UrQMD result with the DLS filter and resolution. The experimental data are taken from ref. [9]. Only the larger systematic error bars are displayed.

**FIG. 7** Model calculations for dilepton spectra from nucleus-nucleus collisions at beam energies of about 1 GeV in comparison to DLS data [8]. The systems  $d+Ca$ ,  $\alpha+Ca$  and  $Ca+Ca$  as well as  $C+C$  have been examined. See figs. 4 and 5 for additional information.

**FIG. 8** Total dilepton spectra from  $Ca+Ca$  collisions compared to two generations of data. To compare to the earlier measurements [42] the old DLS filter V1.5 (dashed line) has been applied. The solid line corresponds to the calculation of fig. 7.

**FIG. 9** Total dilepton spectra from  $Ca+Ca$  collisions with an increased  $\omega$  width. Also shown are effects due to density dependent modifications of the vector meson masses.

Fig. 1

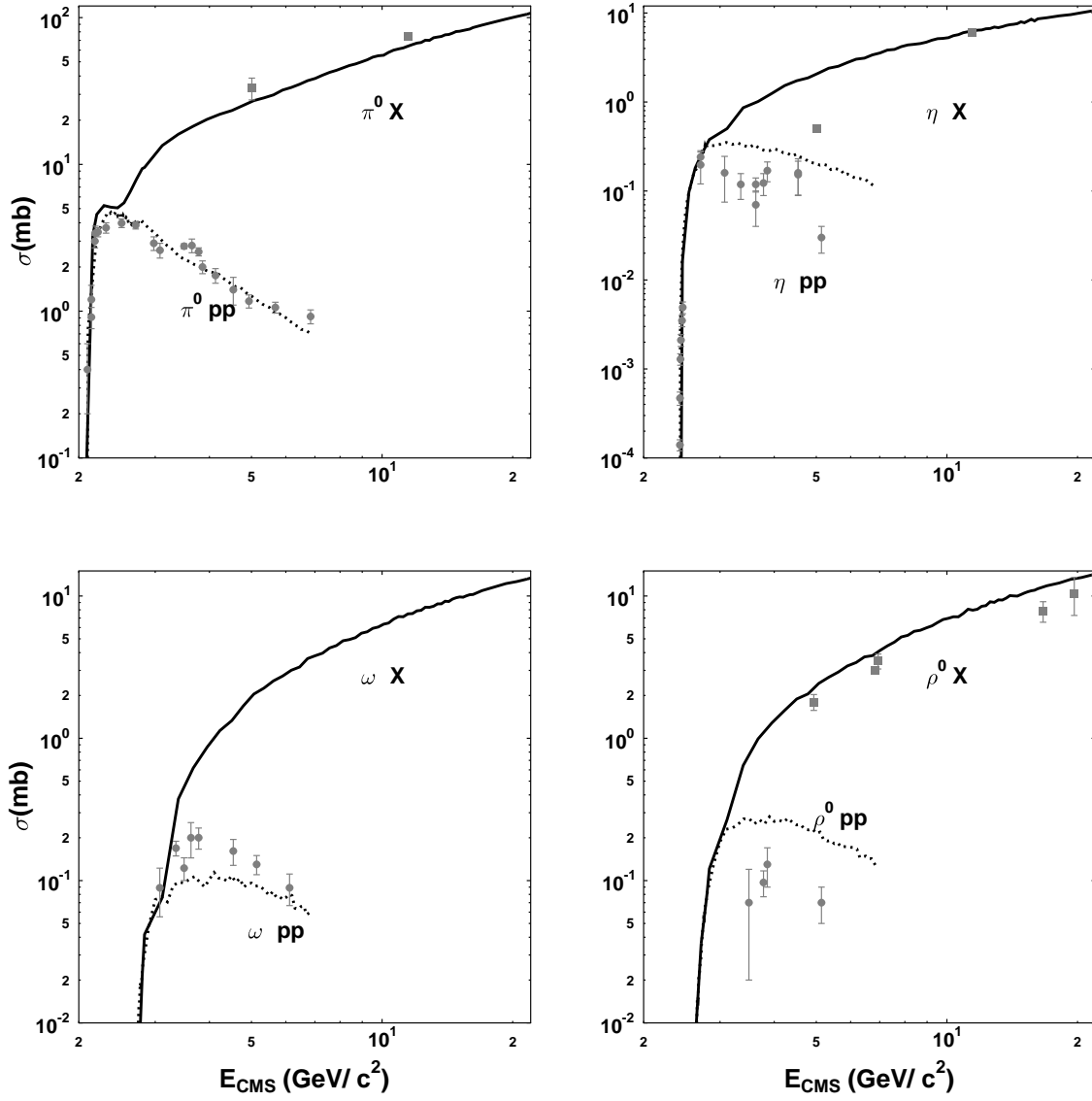


Fig. 2

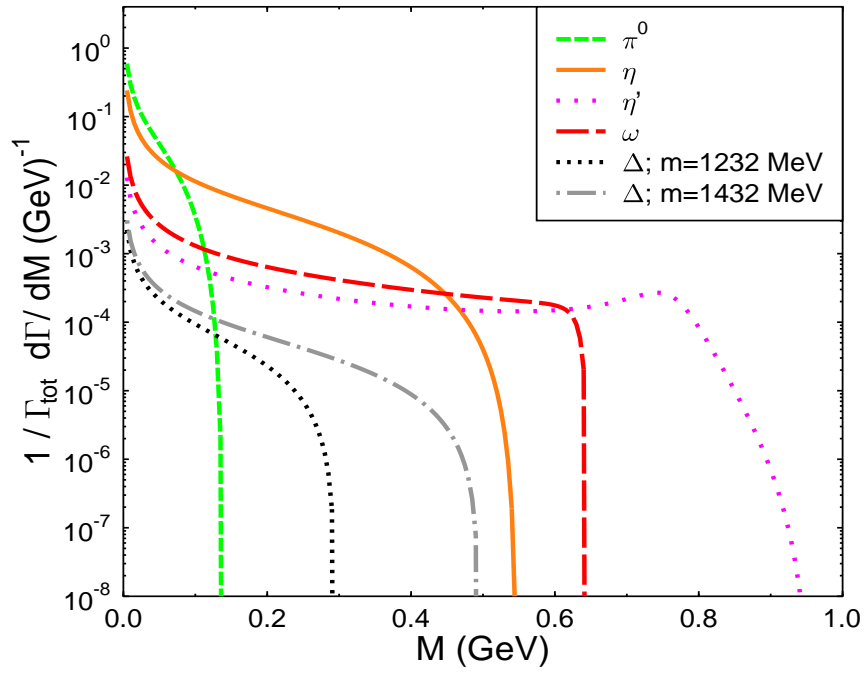


Fig. 3

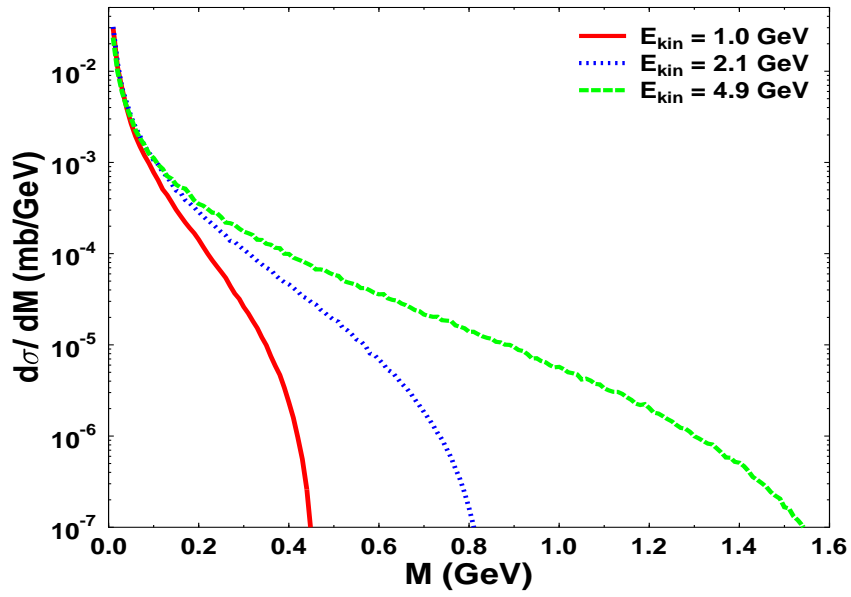


Fig. 4

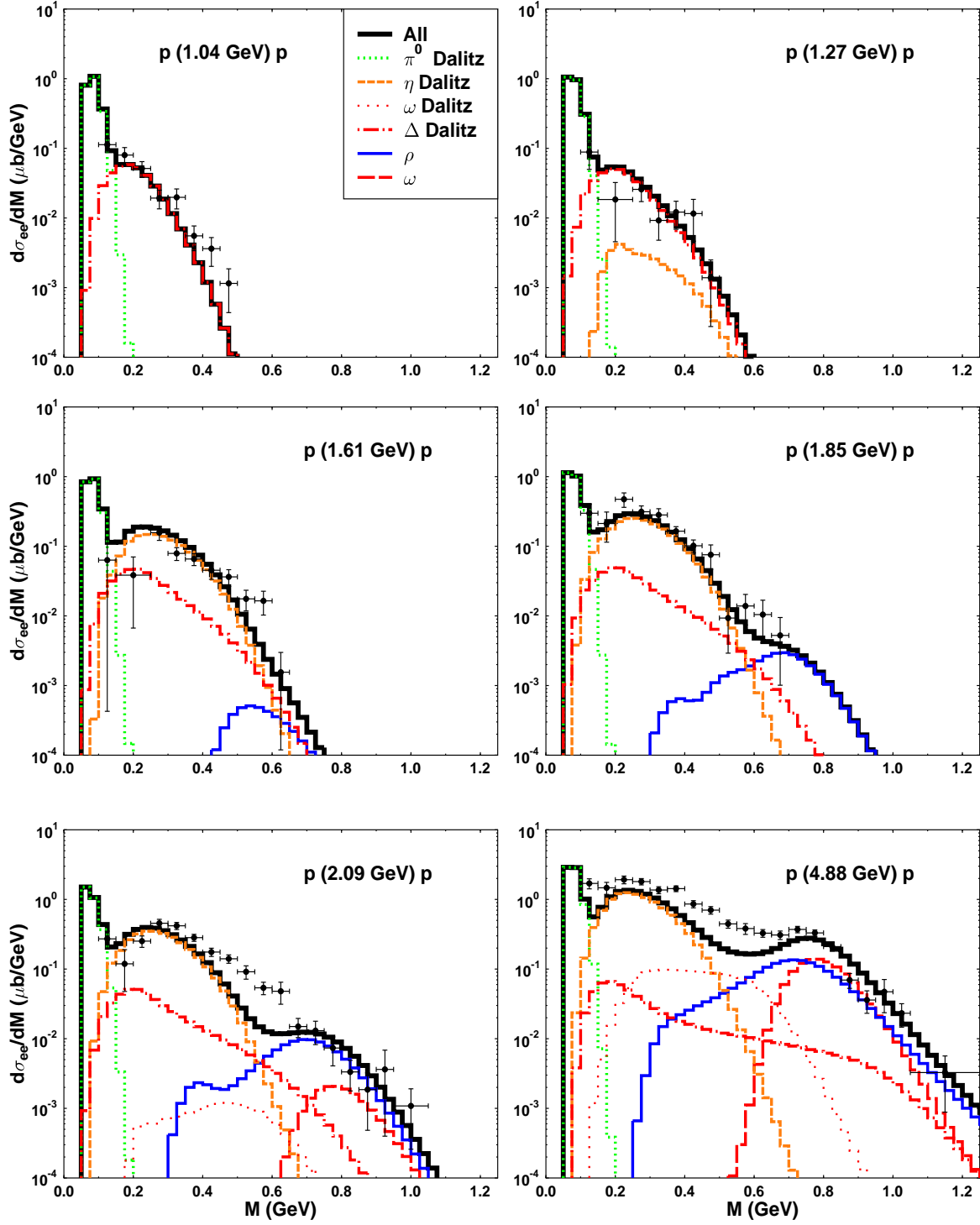


Fig. 5

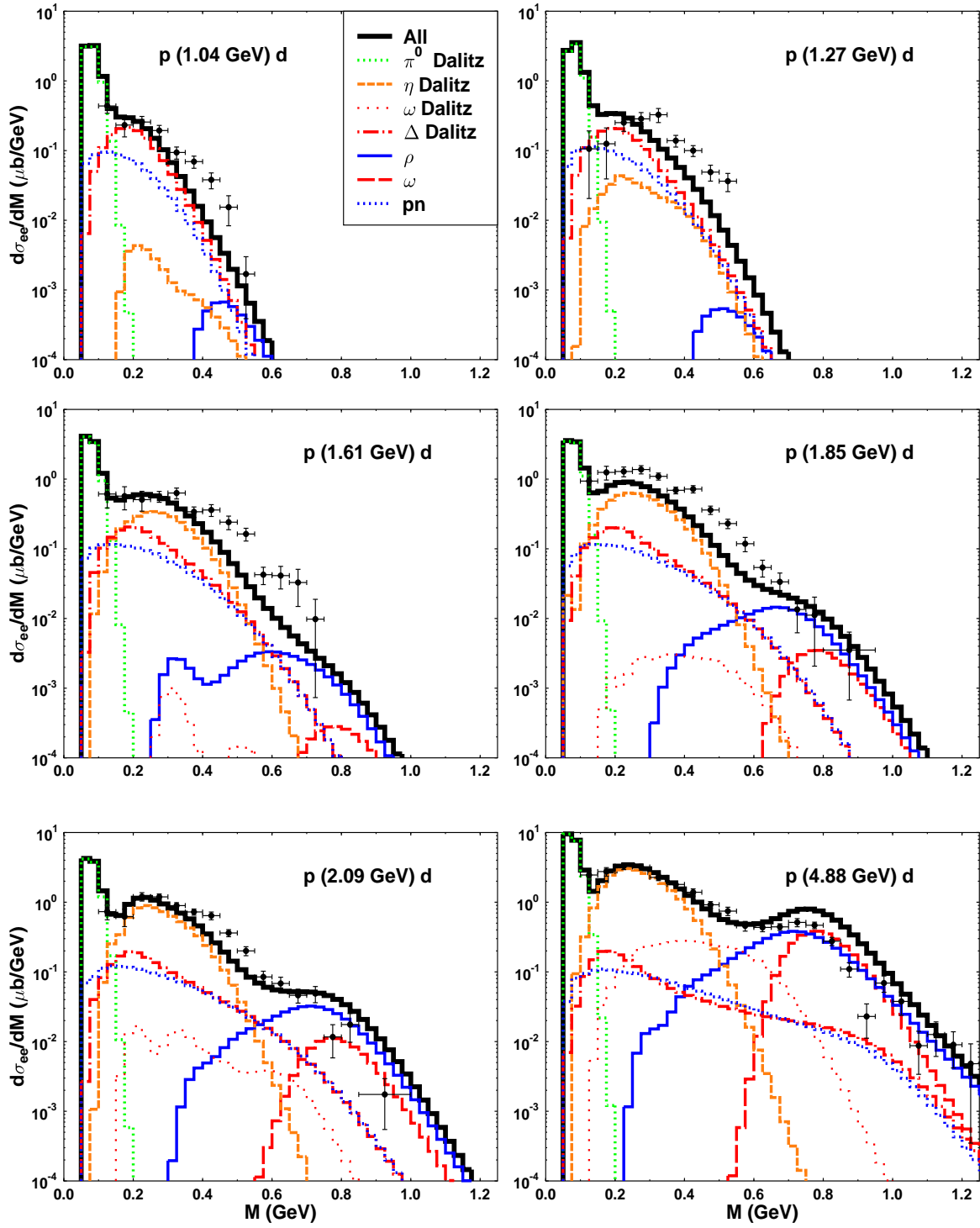
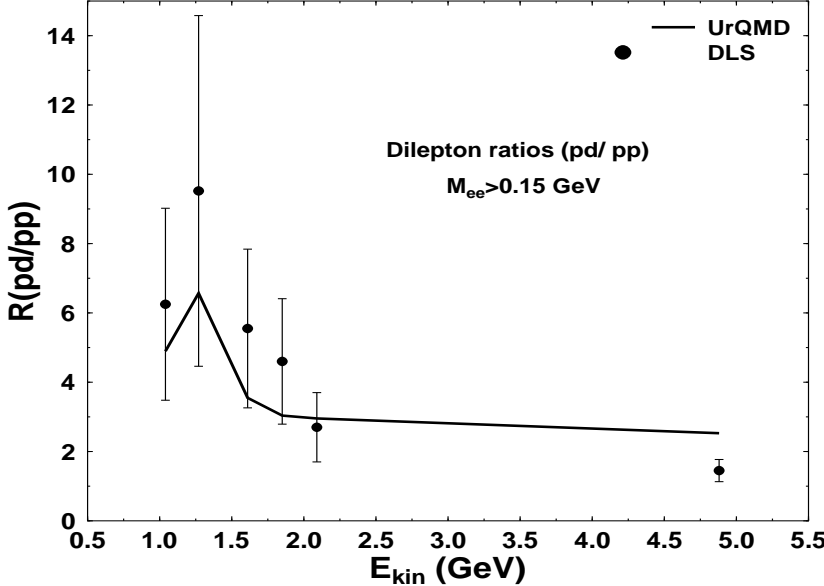


Fig. 6



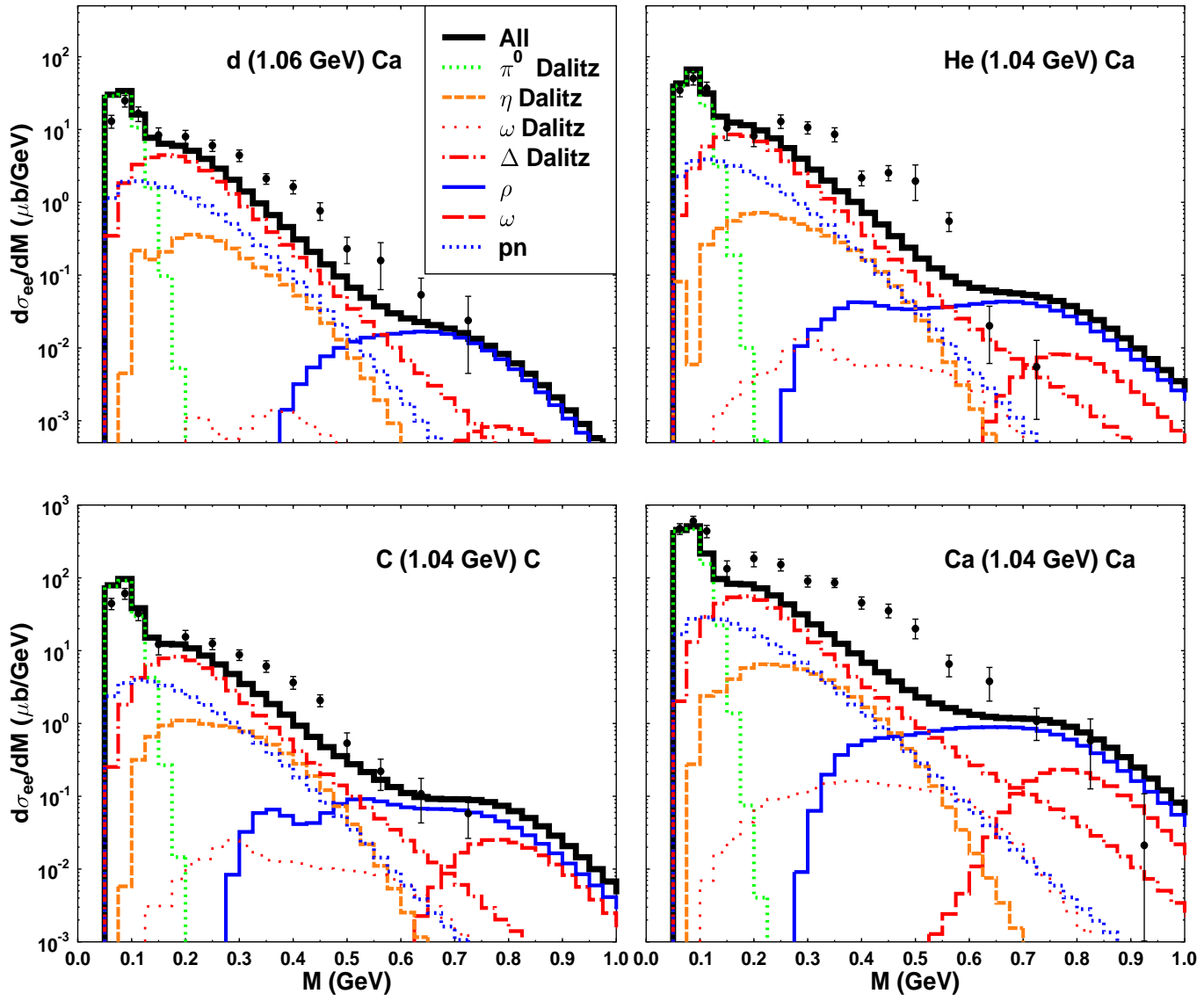


Fig. 7

Fig. 8

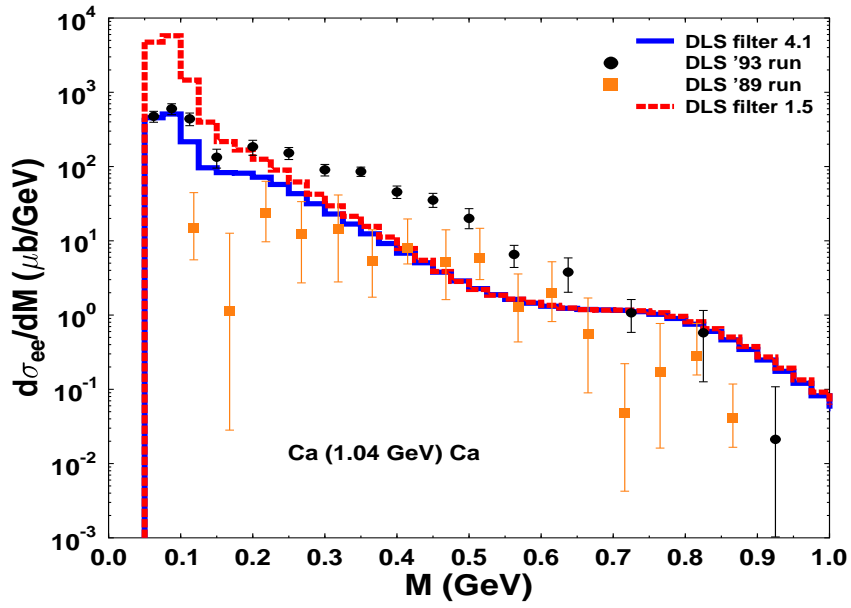


Fig. 9

